SAND2022-1297J

Plasma Sources Science and Technology

ACCEPTED MANUSCRIPT

Measurements of atoms and metastable species in N_2 and H_2-N_2 Ns pulse plasmas

To cite this article before publication: Xin Yang *et al* 2021 *Plasma Sources Sci. Technol.* in press https://doi.org/10.1088/1361-6595/ac3053

Measurements of Atoms and Metastable Species in N_2 and H_2-N_2 Ns Pulse Plasmas

Xin Yang[1,2], Elijah Jans[1], Caleb Richards[1], Sai Raskar[1], Dirk van den Bekerom[1,3], Kai Wu[2], and Igor V. Adamovich[1]

[1] *Nonequilibrium Thermodynamics Laboratory*
Department of Mechanical and Aerospace Engineering
The Ohio State University, Columbus, OH 43210, USA

[2] *State Key Laboratory of Electrical Insulation and Power Equipment,*
Xi'an Jiaotong University, Xi'an, 710049, People's Republic of China

[3] *Combustion Research Facility,*
Sandia National Laboratories, Livermore, CA 94550, USA

Abstract

Time-resolved, absolute number densities of metastable $N_2(A^3\Sigma_u^+,v=0,1)$ molecules, ground state N and H atoms, and rotational-translational temperature have been measured by Tunable Diode Laser Absorption Spectroscopy (TDLAS) and Two-photon Absorption Laser-Induced Fluorescence (TALIF) in diffuse nitrogen and N_2-H_2 plasmas during and after a ns pulse discharge burst. Comparison of the measurement results with the kinetic modeling predictions, specifically the significant reduction of the $N_2(A^3\Sigma_u^+)$ populations and the rate of N atom generation during the burst, suggests that these two trends are related. The slow N atom decay in the afterglow, on the time scale longer than the discharge burst, demonstrates that the latter trend is not affected by N atom recombination, diffusion to the walls, or convection with the flow. This leads to the conclusion that the energy pooling in collisions of $N_2(A^3\Sigma_u^+)$ molecules is a major channel of nitrogen dissociation in electric discharges where a significant fraction of the input energy goes to electronic excitation of N_2. Additional measurements in a 1% H_2-N_2 mixture demonstrate a further significant reduction of $N_2(A^3\Sigma_u^+,v=0,1)$ populations, due to the rapid quenching by H atoms accumulating in the plasma. Comparison with the modeling predictions suggests that the $N_2(A^3\Sigma_u^+)$ molecules may be initially formed in the highly vibrationally excited states. The reduction of the $N_2(A^3\Sigma_u^+)$ number density also diminishes the contribution of the energy pooling process into N_2 dissociation, thus reducing the N atom number density. The rate of N atom generation during the burst also decreases, due to its strong coupling to $N_2(A^3\Sigma_u^+,v)$ populations. On the other hand, the rate of H atom generation, produced predominantly by the dissociative quenching of the excited electronic states of nitrogen by H_2, remains about the same during the burst, resulting in a nearly linear rise of the H atom number density. Comparison of the kinetic model predictions with the experimental results suggests that the yield of H atoms during the quenching of excited electronic state of N_2 by molecular hydrogen is significantly less than 100%. The present results quantify the yield of N and H atoms in high-pressure H_2-N_2 plasmas, which have a significant potential for ammonia generation using plasma-assisted catalysis.

1. Introduction

Diagnostics and predictive modeling of high-pressure nonequilibrium plasmas are essential for the development of efficient plasma chemistry and plasma-assisted catalysis processes. Repetitive nanosecond pulse discharges, sustained at high pulse repetition rates of 1-100 kHz, are readily amenable to their characterization using laser diagnostics, due to their stability at high pressures and scalability to large volumes. In addition, these discharges have considerable potential for engineering applications, due to the efficient generation of reactive atomic species and radicals. Over the last decade, they have been used extensively in plasma flow reactors for studies of plasma-assisted combustion kinetics [1-4]. Number densities of electronically excited metastable species, atoms, radicals, and vibrationally excited molecules are among the major parameters affecting the plasma reactivity and the specific reaction pathways. Although these parameters have been measured in ns pulse discharges previously [1-10], much of this work has been done in relatively complex geometries and for different operating conditions, such that comparison with the modeling predictions and isolating specific molecular energy transfer and plasma transport processes remain rather challenging.

In plasma chemistry experiments, sustaining stable diffuse plasmas at well characterized, reproducible conditions is critical for the analysis and interpretation of the results. Double dielectric barrier, repetitive ns pulse discharges in quasi-one-dimensional, plane-to-plane geometry are attractive in this respect since they generate spatially uniform plasmas at high pressures [1,4]. This greatly simplifies acquiring diagnostic data which require highly reproducible repetitively pulsed experiments, and makes comparison with kinetic modeling predictions straightforward and elucidating. The objective of the present work is to study the fundamental plasma kinetics in this type of discharge sustained in nitrogen and N_2-H_2 mixtures, initially at room temperature, with the main focus on the measurements and modeling predictions of metastable electronically excited $N_2(A^3\Sigma_u^+)$ molecules, N atoms, and H atoms. The present approach is similar to the one used in our recent work [10], with the main focus on the kinetics of $N_2(A^3\Sigma_u^+)$ in high-pressure molecular gas mixtures. In this work, the use of complementary diagnostics and comparison with the modeling predictions is expected to quantify the yield of N and H atoms in these plasmas, with potential applications for plasma-assisted catalysis generation of NH_3 [11,12], and provide new insight into the kinetics of dissociation of molecular nitrogen and hydrogen.

2. Experimental Setup and Kinetic Model

The schematics of the experimental apparatus and laser diagnostics are shown in Fig 1. The plasma is generated in a rectangular cross section quartz channel (16 mm x 8 mm, 10 cm long), fused to a circular quartz tube 1 inch in diameter at both ends. The total length of the tube, with the rectangular cross section in the middle, is 60 cm. The tube is attached to two endpieces, quartz tubes 1 inch in diameter and 8 cm long, via UltraTorr vacuum fittings. Each endpiece has a fused silica optical access window at Brewster's angle at the end. Nitrogen or a nitrogen-hydrogen mixture flows through the cell at the flow rate of 1.0 SLM and pressure of 150 Torr. The combined leak rate of the cell, delivery lines, and exhaust lines is approximately 1.0 Torr/hr, which corresponds to $2.2\cdot10^{-5}$ SLM, i.e. over 4 orders of magnitude lower compared to the flow rate. The estimated upper bound oxygen and water vapor impurity in the flow is $\sim10^{-5}$ and $\sim10^{-6}$ mole fraction, respectively.

The discharge in the cell is produced between two parallel rectangular plate copper electrodes 60 mm long and 12 mm wide, mounted to the top and bottom outside walls of the cell, as shown in Fig. 1. The electrodes are attached to the walls by a silicon rubber adhesive, to prevent corona discharge formation near the electrode surfaces. The discharge is sustained by a FID GmbH FPG 60-100MC4 ns pulse generator (peak voltage 30 kV, pulse duration 10 ns) operated in burst mode at a pulse repetition rate of 100 kHz, burst duration of 5-150 pulses, and burst repetition rate of 10 Hz. The pulse voltage and current waveforms are measured by custom-made, high bandwidth capacitive voltage probes and shunt current probes [13]. Broadband plasma emission images are taken through the side wall of the rectangular section and through one of the Brewster angle windows, using a gated PI-MAX 3 ICCD camera with a UV lens(UV-Nikkor 105 mm f/4.5, Nikon).

A schematic diagram of the Two-photon Absorption Laser-Induced Fluorescence (TALIF) diagnostic, used for the number density measurements of the ground state N(^{4}S) and H(1s^{2}S) atoms generated in the plasma, is shown in Fig. 1(a). For this, a Nd:YAG laser (Continuum, Powerlite 8010) pumps a tunable dye laser (Continuum ND6000) to produce the output at 621 nm (for N TALIF) or 615 nm (for H TALIF). The dye laser output is frequency doubled using a type I BBO crystal, and mixed with the dye laser output to generate a 207 nm beam (for N atom TALIF) or 205 nm beam (for H atom TALIF), separated from the other beams by a Pellin-Broca prism, as shown in Fig. 1(a). A halfwave plate and polarizer combination is used to adjust the laser pulse energy, which is monitored by a calibrated photodiode. During the measurements, the laser energy is maintained within the quadratic TALIF signal range. The laser beam is focused by a 50 cm focal distance lens and directed along the discharge cell. The fluorescence signal is collected through the side wall of the quartz channel, in the direction perpendicular to the beam path, using a 10 cm focal length lens, and detected by a PMT (Hamamatsu R12896) with a gated D-type socket (Hamamatsu C1392), see Fig. 1(a). A slit mask 2 mm wide placed in front of the lens, and a bandpass filter (10 nm bandpass, centered at 750 nm) are used to reduce the emission from the plasma during the N TALIF measurements. A neutral density filter is attached to the PMT, to operate it at the same gain during the absolute calibration of TALIF measurements using krypton, without saturation. The well-known calibration technique is described in detail in Ref. [14].

Fig. 1(b) shows a schematic of the single-pass Tunable Diode Laser Absorption Spectroscopy (TDLAS) diagnostic [10], used for the measurements of $N_2(A^3\Sigma_u^+,v=0,1)$ vibrational level populations in the plasma. Briefly, a tunable diode laser (New Focus Velocity 6312, tuning range from 764 to 781 nm, nominal linewidth < 0.3 MHz) is scanned by varying the voltage on the piezoelectric driver of the laser, with the wavelength monitored continuously during the experiment by a wavemeter (High Finesse WS6-200-IR). The focused laser beam is directed along the discharge cell, with the transmitted beam focused into an optical fiber (Thorlabs BFL22-910) 20 m long to reject the plasma emission, sent to a photodiode detector (Thorlabs DET36A) through a bandpass filter, and monitored by an oscilloscope. The laser scan and data acquisition are controlled by a computer executing a LabView script. To determine whether the partial saturation of the absorption transitions may have an effect on the measurement results, the incident laser beam intensity was attenuated by up to a factor of 30, using a set of neutral density filters placed before the discharge cell. The results show that the laser beam attenuation did not result in a detectable change in the inferred peak $N_2(A^3\Sigma_u^+,v=0)$ number density, indicating that the saturation is a minor effect at the present conditions.

The quasi-zero-dimensional kinetic model used to interpret the experimental data (time-resolved N and H atoms number densities, $N_2(A^3\Sigma_u^+,v)$ populations, and gas temperature) is described in detail in Ref. [10]. Briefly, the model solves the electron energy equation (a moment of the Boltzmann equation), the heavy species energy equation, and equations for the species concentrations. It incorporates the electron impact excitation, dissociation, and ionization processes, state-specific vibrational relaxation of nitrogen, and reactions of excited electronic states of N_2. The time-resolved ns pulse discharge power waveform, used as an input in the model, is obtained from the experimental discharge voltage and current waveforms. The electron impact rate coefficients are predicted by the Boltzmann equation solver Bolsig+ [15], with the cross sections taken from [16,17]. The rates of reactions among the excited electronic states of N_2 are taken from [18-24]. The nascent vibrational distribution of $N_2(A^3\Sigma_u^+,v)$, generated during the collisional quenching of $N_2(B^3\Pi_g)$, is assumed to be the same as inferred from the time-resolved measurements of $N_2(A^3\Sigma_u^+,v=0\text{-}5)$ in our previous work [10].

The rates of conventional chemical reactions in nitrogen-hydrogen mixtures are taken from [12,18,19,22]. The effect of vibrational excitation of the ground electronic state N_2 at the present conditions is shown to be insignificant [10]. However, the kinetic model includes the state-specific vibration-vibration (V-V) and vibration-translation (V-T) energy transfer processes for N_2, with the rate coefficients taken from Refs. [25-29]. In the present work, as in Ref. [10], we assume that N_2 dissociation in the plasma occurs during the energy pooling of two $N_2(A^3\Sigma_u^+)$ molecules,

$$N_2(A^3\Sigma_u^+,v)+N_2(A^3\Sigma_u^+,w)\rightarrow\begin{cases}N_2(B^3\Pi_g)+N_2(X^1\Sigma_g^+)\\ N_2(C^3\Pi_u)+N_2(X^1\Sigma_g^+)\\ N(^4S)+N(^4S)+N_2(X^1\Sigma_g^+)\end{cases}, \quad (1)$$

in addition to electron impact dissociation. Since the rate coefficient of this dissociation channel has not been measured directly, it is treated as an adjustable parameter varied to obtain good agreement with both the TDLAS $N_2(A^3\Sigma_u^+)$ measurements and with TALIF $N(^4S)$ measurements. As shown in Section 3, this assumption results in good agreement with the measurements of N atom number density and $N_2(A^3\Sigma_u^+,v)$ populations. The list of kinetic processes and their rates is given in the supporting information.

3. Results and Discussion

Figure 2 plots the waveforms of voltage, current, instantaneous power, and energy coupled to the capacitive load (i.e. the electrode assembly and the nitrogen plasma) at P = 150 Torr, sustained by a ns pulse train at the repetition rate of 100 kHz. The energy is coupled to the plasma both during the incident voltage pulse and several successive reflected pulses, with the total coupled energy of 3.3 mJ. Figure 3 illustrates the variation of the energy coupled by the incident pulse and the total coupled energy per pulse, for different pulse numbers during a 150-pulse burst 1.5 ms long. It can be seen that the coupled pulse energy remains nearly the same, decreasing by about 10% during the burst. This reduction is likely due to the gradual temperature rise in the plasma during the burst, which reduces the total number density. The coupled pulse energy data taken in nitrogen and H_2-N_2 mixtures with the H_2 mole fraction of 1-20% exhibit the same trend. Increasing the hydrogen mole fraction up to 20% reduces the coupled energy per pulse by 6%, throughout the burst.

Figure 4 shows a collage of single-shot, broadband plasma emission images taken during a 150-pulse discharge burst in nitrogen and a 150-pulse burst in 1% H_2-N_2, both at P=150 Torr. The images are taken both through the side wall of the discharge cell (side view) and through the optical access window at the end of the channel (end view, see Fig. 1), with the camera gate 250 ns long incorporating both the incident pulse and the reflected pulses. From Fig. 4(a), it can be seen that the nitrogen plasma remains diffuse and uniform during the first 100 pulses, with the exception of pulse #1, which exhibits a strongly filamentary structure, due to the low residual ionization remaining from the previous pulse burst generated 100 ms earlier. After pulse #100, diffuse filaments gradually begin to form in the plasma near the electrode edges, most likely due to the onset of the ionization/heating instability. During the entire burst, the plasma remains confined to the region between the electrodes 6 cm long, such that the absorption path for the TDLAS measurements can be determined with an uncertainty of approximately 10%. In 1% H_2-N_2, the plasma filamentation during pulse #1 is more pronounced (see Fig. 4(b)). In this mixture, the onset of the filaments becomes evident during the second half of the burst, near pulse #100 (see Fig. 4(b)).

A dark band clearly visible during pulses #5, #10, and #50, both in nitrogen and H_2-N_2 (see Fig. 4) is formed during the propagation of a plane ionization wave during the discharge gap, as discussed in detail in [30]. The location of the dark band indicates the approximate extent of the wave propagation from the cathode-adjacent wall. In the present measurements, unlike in Ref. [30] the ionization wave does not propagate far across the discharge gap and remains close to the wall near the negative polarity electrode (the bottom wall in Fig. 4), within ≈ 1 mm. This occurs due to the short duration of the incident voltage pulse, approximately 10 ns vs 100 ns in Ref. [30]. At the present conditions, the displacement of the residual electrons by the applied voltage is much smaller, such that the ionization wave formed in the charge separation region near the cathode does not propagate far across the gap, before dissipating in the plasma. Because of this, the coupled energy distribution across the rest of the discharge gap is controlled by the residual electron density distribution from the previous pulse, and remains uniform, as predicted by the quasi-one-dimensional fluid model [30]. This justifies the use of the quasi-zero-dimensional kinetic model for the prediction of the number densities of the excited species and atoms in the present work.

The optical emission spectra from the central region of the plasma, obtained using a mask 2 mm wide, are dominated by the 2nd positive and 1st positive emission bands of molecular nitrogen, as expected. In addition to the spectra, time-resolved emission intensity from these bands during the discharge burst is measured using a gated PMT and narrow bandpass filters, 340 nm center / 12 nm band bass for the dominant $N_2(C^3\Pi_u,v'=0 \rightarrow B^3\Pi_g,v''=0)$ band and 769 nm center / 41 nm bandpass for $N_2(B^3\Pi_g,v'=4\text{-}2 \rightarrow A^3\Sigma_u^+,v''=2\text{-}0)$ bands. As shown in Fig. 5, the emission intensity of the second positive system bands does not vary significantly during the burst, decreasing by 15% over the first 100 pulses and by 30% over the entire 150-pulse burst. The emission intensity of the first positive system bands remains nearly constant during the entire burst (within 5%). Based on these results, along with the measurements of the coupled pulse energy shown in Fig. 3, we conclude that the peak number densities of the excited electronic states of nitrogen produced by electron impact during the discharge burst, $N_2(C^3\Pi_u)$ and $N_2(B^3\Pi_g)$, scale approximately with the discharge pulse energy and do not change significantly. Identifying the dominant factors controlling the variation of the emission intensity of N_2 1st and 2nd positive band systems would require the development of a state-specific collision-radiative model. The gradual increase in the gas temperature, N_2 vibrational level populations, and possibly electron density during the discharge burst may well an effect on the peak $N_2(C^3\Pi_u)$ and $N_2(B^3\Pi_g)$ populations.

Figure 6(a) plots the Kr, N, and H TALIF signal vs. the square laser pulse energy, indicating that in all three cases the laser is operated within the quadratic regime, well below saturation of the absorption transition. During these measurements, the laser pulse energy was varied using a halfwave plate and polarizer combination, as discussed in Section 2. Figure 6(b-d) shows the TALIF scans for these three cases, plotting the convolution of the laser line shape and the absorption line shape, Kr ($5p'[3/2]_2 \rightarrow 5s'[1/2]_1$), N ($3p\ ^4S_{3/2} \rightarrow 3p^4\ S_{1/2,3/2,5/2}$), and H ($1s\ ^2S_{1/2} \rightarrow 3d^2\ S_{3/2,5/2}$), respectively. During the rest of the TALIF measurements, the laser was parked on the respective line center. The transmission curves of the bandpass filters placed in front of the PMT (830 nm center, 20 nm bandpass for Kr; 750 nm center, 10 nm bandpass for N; and 650 nm center, 40 nm bandpass for H) were measured directly, using a calibrated blackbody source. The same approach was used to measure the PMT quantum efficiency ratios at the wavelengths used for N, H, and Kr TALIF. Finally, the two-photon absorption cross sections, radiative lifetimes, and collisional quenching cross sections of the upper states of N, H, and Kr atoms were taken from [14], except for the quenching rate of N by N_2, taken from Ref. [31]. These tests and data, along with the temperature in the plasma, inferred from the TDLAS measurements as discussed below, are sufficient for the absolute calibration of N and H atom measurements.

Figure 7(a,b) plots the time-resolved, absolute $N_2(A^3\Sigma_u^+,v=0,1)$ vibrational level population during a 150-pulse discharge burst, at the conditions of Fig. 4(a), measured by TDLAS. The uncertainty of these measurements, approximately 10%, is controlled mainly by the uncertainty of the absorption path through the plasma. The experimental data (red curve) are compared with the kinetic modeling predictions (blue curve). As discussed in detail in our previous work [10], both the gradual decay of the $N_2(A^3\Sigma_u^+)$ number density during the burst and the increasingly rapid decay after each discharge pulse (i.e. the higher peak-to-valley ratio), evident in Fig. 7, are due to its rapid quenching by N atoms accumulating during the burst,

$$N_2(A^3\Sigma_u^+, v) + N \rightarrow N_2(X^1\Sigma_g^+) + N\,. \qquad (2)$$

This process, along with the energy pooling process of Eq. (1), is the dominant mechanism of $N_2(A^3\Sigma_u^+)$ decay in the nitrogen plasma. From Fig. 7, it can be seen that the modeling predictions are in good agreement with the TDLAS data. However, as discussed below, such agreement can be obtained only when the N_2 dissociation channel during the energy pooling, with a 50% branching ratio, is included in the kinetic model. As stated in our previous work [10], electron impact dissociation alone significantly underestimates the N atom accumulation number density (by about a factor of 2), in which case the model predicts almost no decay of $N_2(A^3\Sigma_u^+)$ during the burst.

Figure 8(a) compares a portion of the TDLAS spectrum of the $N_2(B^3\Pi_g,v'=2 \leftarrow A^3\Sigma_u^+,v''=0)$ band, used for $N_2(A^3\Sigma_u^+,v=0)$ population measurements, with the best fit synthetic spectrum, exhibiting good agreement. The synthetic spectrum was generated using PGOPHER software [32], with the pressure broadening coefficient measured in Ref. [10]. The rotational-translational temperature during a 150-pulse discharge burst in nitrogen at P=150 Torr, inferred from the intensity ratio of $R_{11}(6)$ and $P_{33}(14)$ lines, is plotted in Fig. 8(b). The uncertainty of the temperature measurements is ±10 K. It can be seen that the temperature rise during the burst, due to quenching and relaxation of the excited states generated in the plasma, is less than 100 K, in good agreement with the modeling predictions.

Figure 9 plots the N atom number density measured by TALIF (blue symbols) during a 150-pulse burst in nitrogen, as well as the number density of N atoms generated per discharge

pulse, inferred from these data (red symbols). The number of N atoms generated per pulse is evaluated from the difference between the number densities measured 10 pulses apart. Figure 10(a) also shows the N atom number density vs. the time delay after a 50-pulse discharge burst at these same conditions, illustrating that on the time scale of the discharge burst (0.5-1.5 ms) the N atoms decay by only about 10%. This illustrates that during the burst, the removal of N atoms due to recombination, diffusion to the walls, and convection with the flow, is clearly insignificant. Therefore, the N atom number density measured during the burst is controlled *entirely* by the rate of N_2 dissociation in the plasma, i.e. by the number density of N atoms generated per pulse plotted in Fig. 10(a).

Comparing the $N_2(A^3\Sigma_u^+,v=0,1)$ populations plotted in Fig. 7 and the rate of N atom generation per pulse in Fig. 9, it is readily apparent that they both decrease significantly during the burst, by a factor of 3-5. Note that this occurs at the conditions when both the discharge pulse energy and the emission intensity from the $N_2(C^3\Pi_u)$ and $N_2(B^3\Pi_g)$ states do not exhibit significant variation (see Fig. 5). This strongly suggests that the rate of N_2 dissociation in the plasma is coupled to the $N_2(A^3\Sigma_u^+)$ number density. The effect of highly vibrationally excited molecules in the ground electronic state is unlikely, since the rate of dissociation is highest at the beginning of the burst (see Fig. 9), when the $N_2(X^1\Sigma_g^+,v)$ populations, which accumulate during the burst [10], are still low. Therefore, we have to conclude that N_2 dissociation in the plasma occurs in collisions of two metastable electronic states, both of which are generated in sufficient quantities, otherwise the contribution of this process would be insignificant. Assuming that the dissociation occurs in one of the channels of the energy pooling process of Eq. (1), $N_2(A^3\Sigma_u^+) + N_2(A^3\Sigma_u^+) \rightarrow N(^4S) + N(^4S) + N_2(X^1\Sigma_g^+)$, with the branching ratio of 50%, provides good agreement of the modeling predictions both with the $N_2(A^3\Sigma_u^+,v=0,1)$ population (see Fig. 7) and with the N atom number density during the burst (see Figs. 9,10(a)). The possibility of N_2 dissociation during the energy pooling process of Eq. (1) has been entertained previously, in the kinetic model developed in Ref. [22], based on the measurements of N atom decay in the afterglow. The present results indicate that the branching ratio for this process is significantly higher than was estimated in Ref. [22] (10%). Not including this dissociation process into the kinetic model results in a strong underprediction of the N atom number density and its linear rise during the burst, as well as a significant overprediction of $N_2(A^3\Sigma_u^+,v)$ populations with almost no decay during the burst.

Kinetic modeling also indicates that the apparent effect of decelerating $N(^4S)$ atoms accumulation during the burst may be affected by their "hiding", due to their excitation to the $N(^2P)$ state during the $N_2(A^3\Sigma_u^+)$ quenching,

$$N_2(A^3\Sigma_u^+, v) + N(^4S) \rightarrow N_2(X^1\Sigma_g^+) + N(^2P) , \quad (2a)$$

followed by their decay by associative ionization [33],

$$N(^2P) + N(^2P) \rightarrow N_2^+ + e^- . \quad (3)$$

Including these processes into the model reduces the predicted $N(^4S)$ number density significantly, at variance with the experimental data (see Fig. 10(b)), and also leads to a gradual rise of the electron density predicted during the burst. Quantifying the possible contribution of this reaction pathway at the present conditions would require measurements of the electron density after the discharge burst, vs. the number of pulses in the burst.

Figure 11 plots the $N_2(A^3\Sigma_u^+, v=0,1)$ populations during and after a 150-pulse discharge burst in 1% H_2-N_2 at P=150 Torr. As expected, at these conditions the peak $N_2(A^3\Sigma_u^+)$ populations are significantly lower compared to the measurements in pure nitrogen (see Fig. 7), and they decay much more rapidly. Since the rate of $N_2(A^3\Sigma_u^+)$ quenching by H_2 is very slow [19], this difference is almost certainly due to the rapid $N_2(A^3\Sigma_u^+)$ quenching by H atoms [19], accumulating during the discharge burst. This general trend is reproduced in the kinetic modeling calculations, also plotted in Fig. 11. However, Fig. 11 also illustrates that the model predicts a considerably more rapid rise of $N_2(A^3\Sigma_u^+, v=0,1)$ populations after each discharge pulse, compared to the experimental data. Analysis of the modeling predictions shows that the dominant factor that controls the rise time of $N_2(A^3\Sigma_u^+, v=0,1)$ populations is the nascent vibrational distribution of $N_2(A^3\Sigma_u^+)$ produced during the collisional quenching of the $N_2(B^3\Pi_g)$ state,

$$N_2(B^3\Pi_u, v') + M \rightarrow N_2(A^3\Sigma_u^+, v'') + M \,, \tag{4}$$

followed by the downward vibration-vibration (V-V) exchange with the ground electronic state,

$$N_2(A^3\Sigma_u^+, v) + N_2(X^1\Sigma_g^+, w=0) \rightarrow N_2(A^3\Sigma_u^+, v-2) + N_2(X^1\Sigma_g^+, w=1) \,. \tag{5}$$

The nascent distribution used in the present work was inferred from the time-resolved measurements of the $N_2(A^3\Sigma_u^+, v=0\text{-}5)$ populations, as discussed in detail in our previous work [10]. This distribution is close to the one based on the sums of the Franck-Condon factors for the quenching transitions of Eq. (4), $\sum_{v'=0-7} P(v' \rightarrow v'')$, with additional empirical corrections for v″=0,1. However, the behavior of $N_2(A^3\Sigma_u^+, v''=0,1)$ populations in the N_2-H_2 mixture (specifically, a much lower "peak-to-valley" ratio) suggests that at the present conditions the nascent vibrational distribution heavily favors the high vibrational levels, v″=6,7, with much lower initial populations of v″=0,1. In this case, the rise of $N_2(A^3\Sigma_u^+, v''=0,1)$ populations, controlled by the V-V exchange of Eq. (5), is far more gradual, and the peak populations are significantly lower, due to the rapid $N_2(A^3\Sigma_u^+, v''=0,1)$ quenching by H and N atoms during the V-V cascade. The populations predicted using this "top-heavy" nascent vibrational distribution, plotted in Fig. 12, are much closer to the experimental data. Fig. 13(a) compares the two vibrational distributions used for comparison with the modeling predictions in the present work, the "baseline" distribution used in Ref. [10] and the "top-heavy" distribution weighted toward v=6,7.

The likely explanation why the nascent $N_2(A^3\Sigma_u^+)$ vibrational distribution at the present conditions may favor the high vibrational levels is that the voltage rise time of the pulse generator used in the present work (FID 60-100MC4) is considerably shorter compared to that in Ref. [10] (MegaImpulse NPG-18/100k), as illustrated in Fig. 13(b). This, as well as a shorter electrode gap (8 mm compared to 10 mm in Ref. [10]) results in (i) higher peak reduced electric field (E/N), electron temperature, and electron density achieved in the discharge gap, and (ii) shorter plasma self-shielding time, controlled by the ionization wave propagation across the gap [30]. Because of this, at the present conditions the energy is coupled to the plasma over a shorter time period, at a higher peak E/N and electron temperature, likely resulting in population of higher vibrational levels of excited electronic states of N_2, including $N_2(B^3\Pi_g)$ and $N_2(A^3\Sigma_u^+)$. Although this explanation is plausible, it is not clear why the kinetic model with the baseline nascent vibrational distribution of $N_2(A^3\Sigma_u^+)$ yields good agreement with the present data in pure nitrogen (see Fig. 7), while exhibiting such a significant difference in a 1% H_2-N_2 mixture (see Fig. 11). In addition, the modeling predictions using the "top-heavy" nascent vibrational distribution of $N_2(A^3\Sigma_u^+)$ in

pure nitrogen are at variance with the experimental data. The reason for this difference remains not understood, and requires additional measurements of the nascent vibrational populations of $N_2(A^3\Sigma_u^+)$ for different voltage pulse waveforms.

Figure 14 plots the experimental and predicted (a) N atom and (b) H atom number densities during a 150-pulse burst in 1% H_2-N_2 at P=150 Torr. The number of N atoms generated per pulse, inferred from the time-resolved N atom number density data, is also shown in Fig. 14(a). Comparison of the N and H atom number densities exhibits a striking difference, indicating that the N atom production rate decreases during the burst, while the rate of H atom production remains about the same, such that they continue to accumulate approximately linearly during the burst. Analysis of the kinetic modeling predictions shows that the dominant process of H atom generation in the plasma at the present conditions is the dissociative quenching of excited electronic states of N_2 by H_2 molecules,

$$N_2(B^3\Pi_u,\ C^3\Pi_u,\ a'^1\Sigma_u^-) + H_2 \rightarrow N_2(X^1\Sigma_g^+) + H + H. \quad (6)$$

Assuming that the yield of H atoms in the processes of Eq. (6) is 1, i.e. that every quenching collision results in H_2 dissociation, overpredicts the H atom number density by approximately a factor of two. Reducing the H atom yield to 0.5 results in much better agreement with the data (see Fig. 14(b)). This suggests a significant contribution of the non-dissociative cascade quenching of the excited electronic states of N_2 in collisions with H_2, most likely to $N_2(A^3\Sigma_u^+)$, for which the quenching rate coefficient is fairly slow [19].

The decay of N and H atoms after a 50-pulse discharge burst in 1% H_2-N_2 at P=150 Torr is illustrated in Fig. 15. In both cases, the atom number density remains nearly the same for up to 1 ms after the burst, decaying by about 15% in each case. Similar to the data taken in pure nitrogen (see Fig. 10(a)), this demonstrates that the number densities of the ground state atoms during the discharge burst (for at least up to 50 pulses) are controlled entirely by the rates of their production in the plasma, and are not sensitive to the decay processes (recombination, wall diffusion, and convection with the flow). From Fig. 15(a), it can be seen that the rate of decay of N atoms in the afterglow is overpredicted by the kinetic model, most likely due to the overprediction of the H atom number density (see Fig. 15(b)), which leads to a higher rate of the atom recombination reaction, N + H + M ⟶ NH + M.

Finally, Fig. 16 shows the variation of N and H atom number densities after a 50-pulse discharge burst at P=150 Torr with the hydrogen mole fraction in the N_2-H_2 mixtures at P=150 Torr. It can be seen that adding even a small amount of hydrogen, 1%, results in a significant reduction of the N atom number density, by a factor of 4. Comparison with the modeling predictions indicates that this occurs primarily due to the rapid quenching of $N_2(A^3\Sigma_u^+)$ molecules by H atoms generated in the plasma, which diminishes the contribution of the energy pooling of Eq. (1) into nitrogen dissociation. Further increase of the H_2 fraction in the mixture leads to a more gradual reduction of the N atom number density, while the H atom concentration continues to increase. This trend is in good agreement with the modeling predictions, which illustrate that H atoms are generated predominantly by the reactive quenching of the excited electronic states of N_2, although the contribution of the direct electron impact dissociation does increase with the H_2 mole fraction. It can be seen that in mixtures with a significant H_2 fraction, 20-30%, the H atom number density exceeds that of the N atoms by about an order of magnitude, making it the most dominant species in the mixture. Although the kinetic model reproduces this trend, it also

overpredicts the N and H atom number densities in H_2-N_2 mixtures with the hydrogen fraction exceeding 1%, by up to a factor of 2. This illustrates that the predictive capability of the kinetic model over a wide range of operating conditions remains rather limited, and its verification by the experimental data is critical.

4. Summary

In the present work, time-resolved, absolute number densities of metastable $N_2(A^3\Sigma_u^+,v=0,1)$ molecules, ground state N and H atoms, and rotational-translational temperature are measured by TDLAS and TALIF in nitrogen and N_2-H_2 plasmas during and after a ns pulse discharge burst, at a high pulse repetition rate. At these conditions, the discharge pulse energy coupled to the plasma, as well as the number densities of electronically excited $N_2(C^3\Pi_u)$ and $N_2(B^3\Pi_g)$ molecules, remains approximately the same during the burst. The nitrogen plasma remains diffuse during the entire burst, although in N_2-H_2, filaments begin to develop during the latter half of the burst. This justifies using a quasi-zero-dimensional kinetic model for the analysis of the kinetic processes in the plasma.

Comparison of the measurement results with the kinetic modeling predictions, specifically the significant reduction of both the $N_2(A^3\Sigma_u^+,v=0,1)$ populations and the rate of N atom generation during the discharge burst, strongly suggests that these two well-reproduced trends are related. The slow N atom decay in the afterglow, on the time scale longer than the discharge burst, demonstrates that the latter trend is not affected by N atom recombination, diffusion to the walls, or convection with the flow. This leads us to conclude that the energy pooling in collisions of metastable $N_2(A^3\Sigma_u^+)$ molecules is a major channel of nitrogen dissociation in electric discharges where a significant fraction of the input energy goes to electronic excitation of molecular nitrogen. Without this assumption, the kinetic model would (i) strongly underpredict the rate of N atom generation and the trend for its reduction during the burst, and (ii) overpredict the $N_2(A^3\Sigma_u^+,v)$ populations while strongly underpredicting their gradual decay during the burst. Assuming that N_2 dissociation occurs in collisions of $N_2(A^3\Sigma_u^+)$ molecules, with a 50% yield, results in good agreement with the experimental data in nitrogen. The dynamics of N_2 dissociation in collisions of electronically excited metastable molecules, suggested in the present work, is not understood. Although the excitation of $N_2(C^3\Pi_u)$ and $N_2(B^3\Pi_g)$ states during the energy pooling reaction of Eq. (1) has been demonstrated over three decades ago [34,35], the effect of predissociation of the high vibrational levels of these states, as well as the single electronic states above the dissociation level, on the N atom yield remains a matter of discussion [36,37]. In quasi-steady-state electric discharges (such as those sustained by DC and RF voltage waveforms at a significantly lower reduced electric field), where most of the input energy goes to vibrational excitation of N_2 in the ground electronic state, the role of this dissociation mechanism may well be less significant. At the present conditions, highly vibrationally excited N_2 molecules in the ground electronic state N_2 are unlikely to affect the $N_2(A^3\Sigma_u^+)$ kinetics, due to the relatively low discharge energy fraction going to vibrational excitation and the rapid $N_2(A)$ quenching by N atoms.

Additional measurements in a 1% H_2-N_2 mixture demonstrate a further significant reduction of $N_2(A^3\Sigma_u^+,v=0,1)$ populations, due to the rapid quenching by H atoms accumulating in the plasma. Comparison of the time-resolved $N_2(A^3\Sigma_u^+,v=0,1)$ populations with the modeling predictions suggest that the $N_2(A^3\Sigma_u^+)$ molecules are initially formed in highly vibrationally excited states. The reduction of the $N_2(A^3\Sigma_u^+)$ number density also diminishes the contribution of

the energy pooling process into N_2 dissociation, such that the N atom number density decreases by approximately a factor of 4. The rate of N atom generation during the burst also decreases, due to its strong coupling to $N_2(A^3\Sigma_u^+,v)$ populations. On the other hand, the rate of H atom generation, produced predominantly by the dissociative quenching of the excited electronic states of nitrogen by H_2, remains about the same during the burst, resulting in a nearly linear rise of the H atom number density. Comparison of the kinetic model predictions with the experimental results suggests that the yield of H atoms during the quenching of excited electronic state of N_2 by molecular hydrogen is significantly less than 100%. Reducing the yield to 50% results in a good agreement between the H TALIF measurements and the modeling predictions in the 1% H_2-N_2 mixture. However, the model still overpredicts the N and H atom number densities in H_2-N_2 mixtures with the hydrogen fraction exceeding 1%, by up to a factor of 2, indicating somewhat limited predictive capability over a wide range of conditions.

The present results quantify the yield of N and H atoms generated in repetitive ns pulse discharges sustained in high-pressure H_2-N_2 mixtures, which will be used for the further analysis of plasma-assisted catalysis generation of ammonia.

5. Acknowledgments

The support of US DOE Collaborative Research Center for Studies of Plasma-Assisted Combustion and Plasma Catalysis and the China Scholarship Council (No. 201906280082) is gratefully acknowledged. We would also like to thank Dr. Nikolay Popov from Moscow State University, Russia, for helpful and productive discussions.

References

1. Z. Yin, I.V. Adamovich, and W.R. Lempert, "OH Radical and Temperature Measurements During Ignition of H_2-Air Mixtures Excited by a Repetitively Pulsed Nanosecond Discharge", *Proceedings of the Combustion Institute* 34 (2013) 3249
2. J.K. Lefkowitz, M. Uddi, B.C. Windom, G. Lou, and Y. Ju, "In situ species diagnostics and kinetic study of plasma activated ethylene dissociation and oxidation in a low temperature flow reactor", *Proceedings of the Combustion Institute* 35 (2015) 3505
3. N. Tsolas, J.G. Lee, and R.A. Yetter, "Flow reactor studies of non-equilibrium plasma-assisted oxidation of n-alkanes", *Philosophical Transactions of the Royal Society A* 373 (2015) 20140344
4. C. Winters, Z. Eckert, Z. Yin, K. Frederickson, and I.V Adamovich, "Measurements and Kinetic Modeling of Atomic Species in Fuel-Oxidizer Mixtures Excited by a Repetitive Nanosecond Pulse Discharge", *Journal of Physics D: Applied Physics* 51 (2018) 015202
5. G.D. Stancu, M. Janda, F. Kaddouri, D.A. Lacoste, and C.O. Laux, "Time-Resolved CRDS Measurements of the $N_2(A^3\Sigma_u^+)$ Density Produced by Nanosecond Discharges in Atmospheric Pressure Nitrogen and Air", *Journal of Physical Chemistry A* 114 (2010) 201
6. G.D. Stancu, F. Kaddouri, D.A. Lacoste, and C.O. Laux, "Atmospheric pressure plasma diagnostics by OES, CRDS and TALIF", *Journal of Physics D: Applied Physics*. 43 (2010) 124002

7. A. Montello, Z. Yin, D. Burnette, I.V. Adamovich, and W.R Lempert, "Picosecond CARS Measurements of Nitrogen Vibrational Loading and Rotational/Translational Temperature in Nonequilibrium Discharges", *Journal of Physics D: Applied Physics* 46 (2013) 464002
8. A. Lo, A. Cessou, P. Boubert and P. Vervisch, "Space and time analysis of the nanosecond scale discharges in atmospheric pressure air: I. Gas temperature and vibrational distribution function of N_2 and O_2", *Journal of Physics D: Applied Physics* 47 (2014) 115201
9. D. Burnette, A. Montello, I.V. Adamovich, and W.R. Lempert, "Nitric Oxide Kinetics in the Afterglow of a Diffuse Plasma Filament", *Plasma Sources Science and Technology* 23 (2014) 045007
10. E.R. Jans, S. Raskar, X. Yang, and I.V. Adamovich, "Kinetics of Metastable $N_2(A^3\Sigma_u^+,v)$ Molecules in High-Pressure Nonequilibrium Plasmas", *Plasma Sources Science and Technology* 30 (2021) 025003
11. P. Mehta, P. Barboun, F.A. Herrera, J. Kim, P. Rumbach, D.B. Go, J.C. Hicks, and W.F. Schneider, "Overcoming ammonia synthesis scaling relations with plasma-enabled catalysis", *Nature Catalysis* 1 (2018) 269
12. J. Shah, W. Wang, A. Bogaerts, and M.L. Carreon, "Ammonia Synthesis by Radio Frequency Plasma Catalysis: Revealing the Underlying Mechanisms", *ACS Applied Energy Materials* 1 (2018) 4824
13. K. Takashima, Z. Yin, and I.V. Adamovich, "Measurements and Kinetic Modeling of Energy Coupling in Volume and Surface Nanosecond Pulse Discharges", *Plasma Sources Science and Technology* 22 (2013) 015013
14. K. Niemi, V. Schulz-von der Gathen, and H. F. Döbele, "Absolute calibration of atomic density measurements by laser-induced fluorescence spectroscopy with two-photon excitation", *Journal of Physics D: Applied Physics* 34 (2001) 2330
15. G.J.M. Hagelaar and L.C. Pitchford, "Solving the Boltzmann Equation to Obtain Electron Transport Coefficients and Rate Coefficients for Fluid Models", *Plasma Sources Science and Technology* 14 (2005) 722-733
16. Morgan database, www.lxcat.net, 2016
17. P.C. Cosby, "Electron-impact dissociation of nitrogen", *Journal of Chemical Physics* 98 (1993) 9544
18. I.A. Kossyi, A.Yu. Kostinsky, A.A. Matveyev, V.P. Silakov, "Kinetic Scheme of the Non-equilibrium Discharge in Nitrogen-Oxygen Mixtures", *Plasma Sources Science and Technology* 1 (1992) 207
19. J.T. Herron, "Evaluated Chemical Kinetics Data for Reactions of $N(^2D)$, $N(^2P)$, and $N_2(A^3\Sigma_u^+)$ in the Gas Phase", *Journal of Physical and Chemical Reference Data* 28 (1999) 1453
20. N.A. Popov, "Vibrational kinetics of electronically-excited $N_2(A^3\Sigma,v)$ molecules in nitrogen discharge plasma", *Journal of Physics D: Applied Physics* 46 (2013) 355204
21. L.G. Piper, "Energy transfer studies on $N_2(X,v)$ and $N_2(B^3\Pi_g)$", *Journal of Chemical Physics* 97 (1992) 270
22. B. Gordiets, C.M. Ferreira, M.J. Pinheiro, and A. Ricard, "Self-consistent kinetic model of low-pressure flowing discharges: I. Volume processes", *Plasma Sources Science and Technology* 7 (1998) 363

23. S.V. Pancheshnyi, S.M. Starikovskaia and A.Yu. Starikovskii, "Collisional deactivation of $N_2(C^3\Pi_u, v=0, 1, 2, 3)$ states by N_2, O_2, H_2 and H_2O molecules", *Chemical Physics* 262 (2000) 349
24. N.A. Popov, "Effect of a pulsed high-current discharge on hydrogen-air mixtures", *Plasma Physics Reports* 34 (2008) 376
25. S. Lanier, I. Shkurenkov, I. V. Adamovich, and W. R. Lempert. "Two-stage energy thermalization mechanisms in nanosecond pulse discharges in air and hydrogen-air mixtures", *Plasma Sources Science and Technology* 24 (2015) 025005
26. T. Ahn, I. V. Adamovich, and W. R. Lempert. "Determination of nitrogen V-V transfer rates by stimulated Raman pumping", *Chemical Physics* 289 (2004) 233
27. F. Esposito, I. Armenise and M. Capitelli, "N-N_2 state to state vibrational-relaxation and dissociation rates based on quasiclassical calculations", *Chemical Physics* 331 (2006) 1
28. R.J. McNeal, M.E. Whitson, G.R. Cook, "Quenching of vibrationally excited N_2 by atomic oxygen", *Chemical Physics Letters* 16 (1972) 507
29. D.C. Allen, E.T. Chandler, E.A. Gregory, R.M. Siddles, C.J.S.M. Simpson, "Vibrational deactivation of $N_2(v = 1)$ by n-H_2 and by p-H_2 in the temperature range 300-80 K", *Chemical Physics Letters* 76 (1980) 347
30. K. Orr, X. Yang, I. Gulko, and I.V. Adamovich, "Formation and Propagation of Ionization Waves During Ns Pulse Breakdown in Plane-to-Plane Geometry", *Plasma Sources Science and Technology* 29 (2020) 125022
31. S.F. Adams, T.A. Miller, "Two-photon absorption laser-induced fluorescence of atomic nitrogen by an alternative excitation scheme", *Chemical Physics Letters* 295 (1998) 305
32. PGOPHER, A Program for Simulating Rotational, Vibrational and Electronic Spectra, C. M. Western, *Journal of Quantitative Spectroscopy and Radiative Transfer* 186 (2016) 221
33. N. A. Popov, "Associative Ionization Reactions Involving Excited Atoms in Nitrogen Plasma", Plasma Physics Reports 35 (2009) 436
34. L.G. Piper, "State-to-state $N_2(A^3\Sigma_u^+)$ energy-pooling reactions. I. The formation of $N_2(C^3\Pi_u)$ and the Herman infrared system", *Journal of Chemical Physics* 88 (1988) 231
35. L.G. Piper, "State-to-State $N_2(A^3\Sigma_u^+)$ energy-pooling reactions. II. The formation and quenching of $N_2(B^3\Pi_g, v' = 1\text{-}12)$", *Journal of Chemical Physics* 88 (1988) 6911
36. N.A. Popov, "Dissociation of Nitrogen in a Pulse-Periodic Dielectric Barrier Discharge at Atmospheric Pressure", *Plasma Physics Reports* 39 (2013) 420
37. A.V. Volynets, D.V. Lopaev, T.V. Rakhimova, A.A. Chukalovsky, Yu.A. Mankelevich, N.A. Popov, A.I. Zotovich, and A.T. Rakhimov, "N_2 dissociation and kinetics of $N(^4S)$ atoms in nitrogen DC glow discharge", *Journal of Physics D: Applied Physics* 51 (2018) 364002

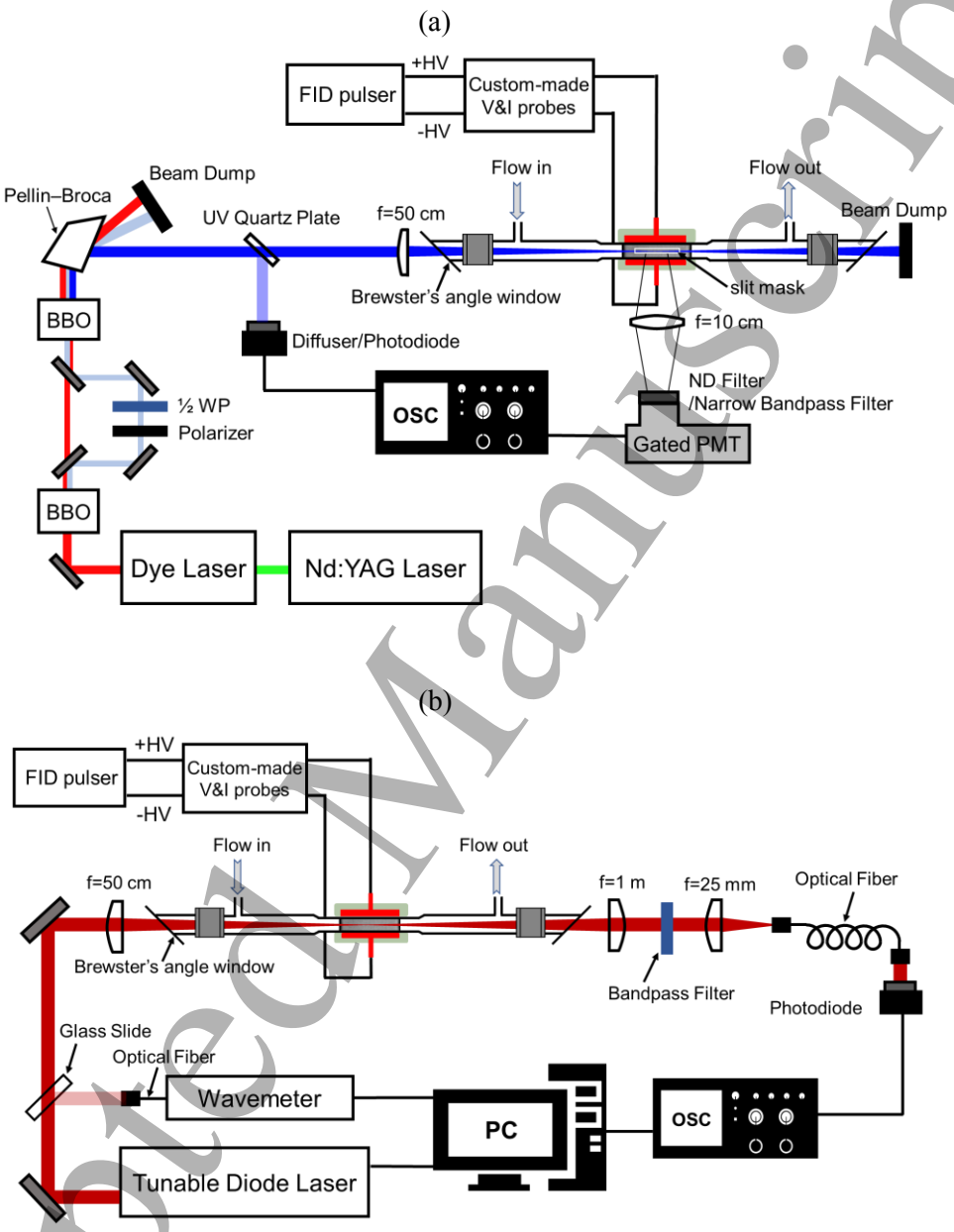

Figure 1. Schematic diagram of the discharge cell and laser diagnostics, (a) Two-photon Absorption Laser-Induced Fluorescence (TALIF), and (b) Tunable Diode Laser Absorption Spectroscopy (TDLAS).

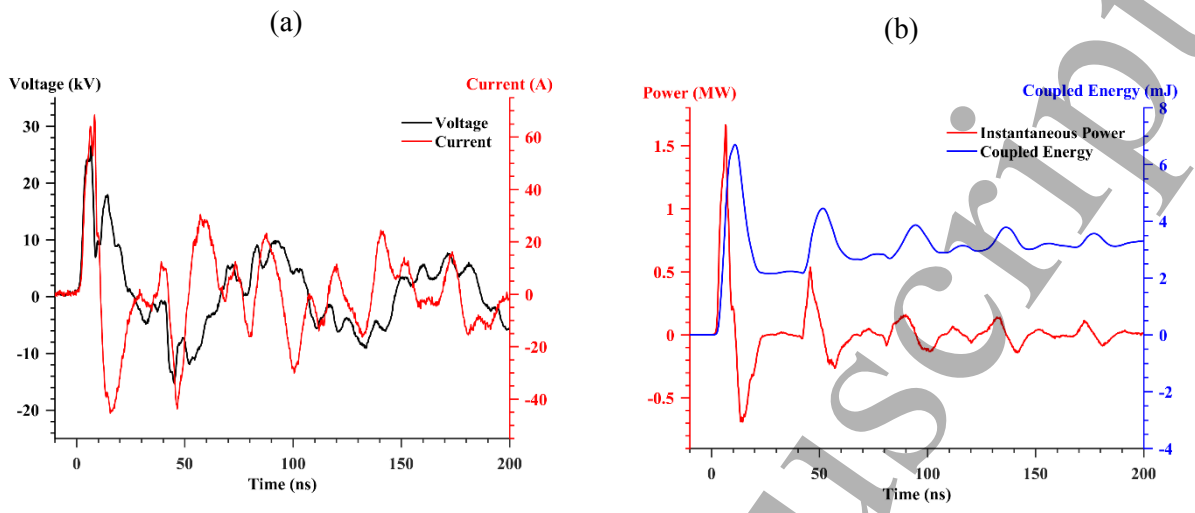

Figure 2. (a) Voltage and current waveforms, (b) instantaneous power and coupled energy waveforms in a ns pulse discharge in nitrogen at P=150 Torr, pulse repetition rate of 100 kHz, and burst repetition rate of 10 Hz (pulse #50 in a 150-pulse burst).

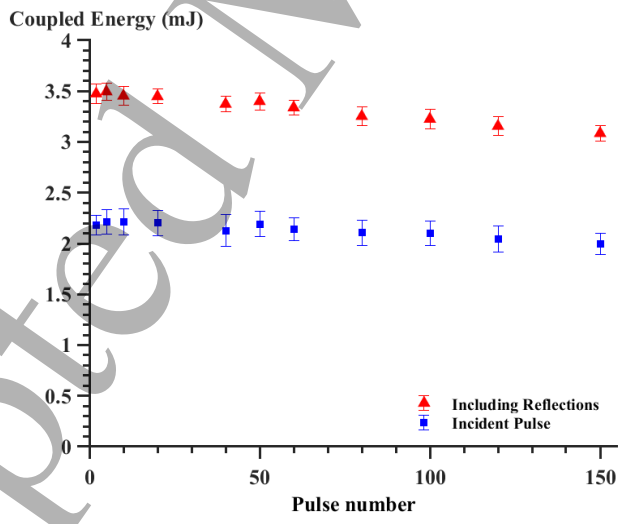

Figure 3. Energy coupled by the incident pulse (blue squares, measured at t= 30 ns) and total coupled energy per pulse (red triangles, measured at t = 200 ns) during a 150-pulse burst in nitrogen at P=150 Torr, at a pulse repetition rate of 100 kHz and burst repetition rate of 10 Hz. Error bars indicated standard deviations of the measurements taken over 100 bursts.

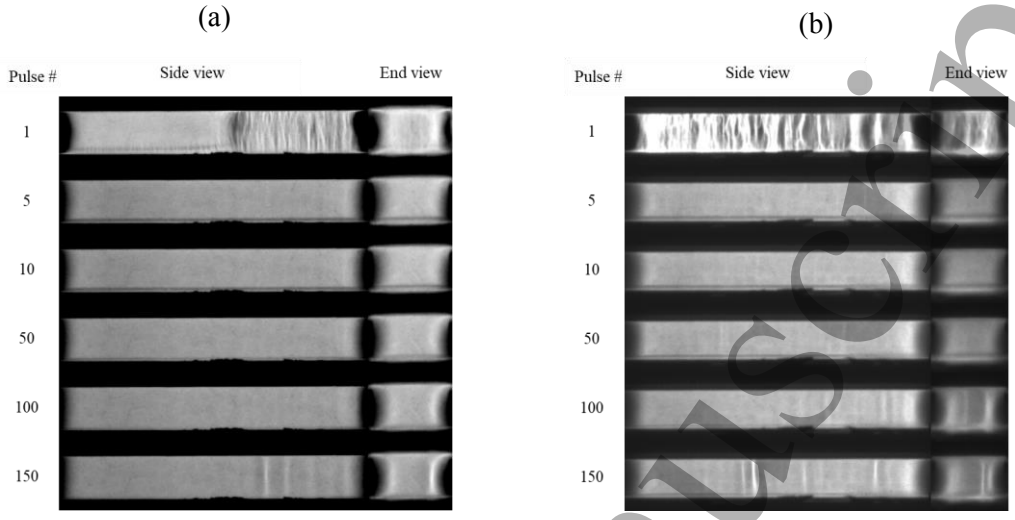

Figure 4. Single-shot, broadband plasma emission images taken during the discharge burst, at the pulse repetition rate of 100 kHz and burst repetition rate of 10 Hz, side view and end view: (a) nitrogen, P=150 Torr, 150-pulse burst; (b) 1% H_2-N_2 mixture, P=150 Torr, 150-pulse burst. Camera gate 250 ns.

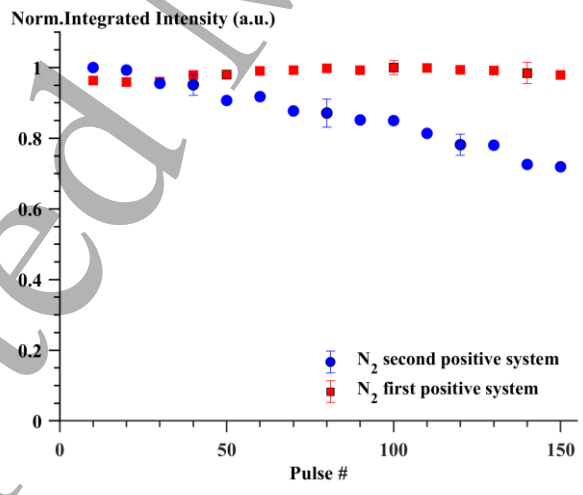

Figure 5. $N_2(C^3\Pi_u,v'=0 \longrightarrow B^3\Pi_g,v''=0)$ and $N_2(B^3\Pi_g,v'=4\text{-}2 \rightarrow A^3\Sigma_u^+,v''=2\text{-}0)$ emission intensity measured by a gated PMT with bandpass filters during a 150-pulse discharge burst in nitrogen with a PMT gate of 1 μs. Error bars indicated standard deviations of multiple measurements.

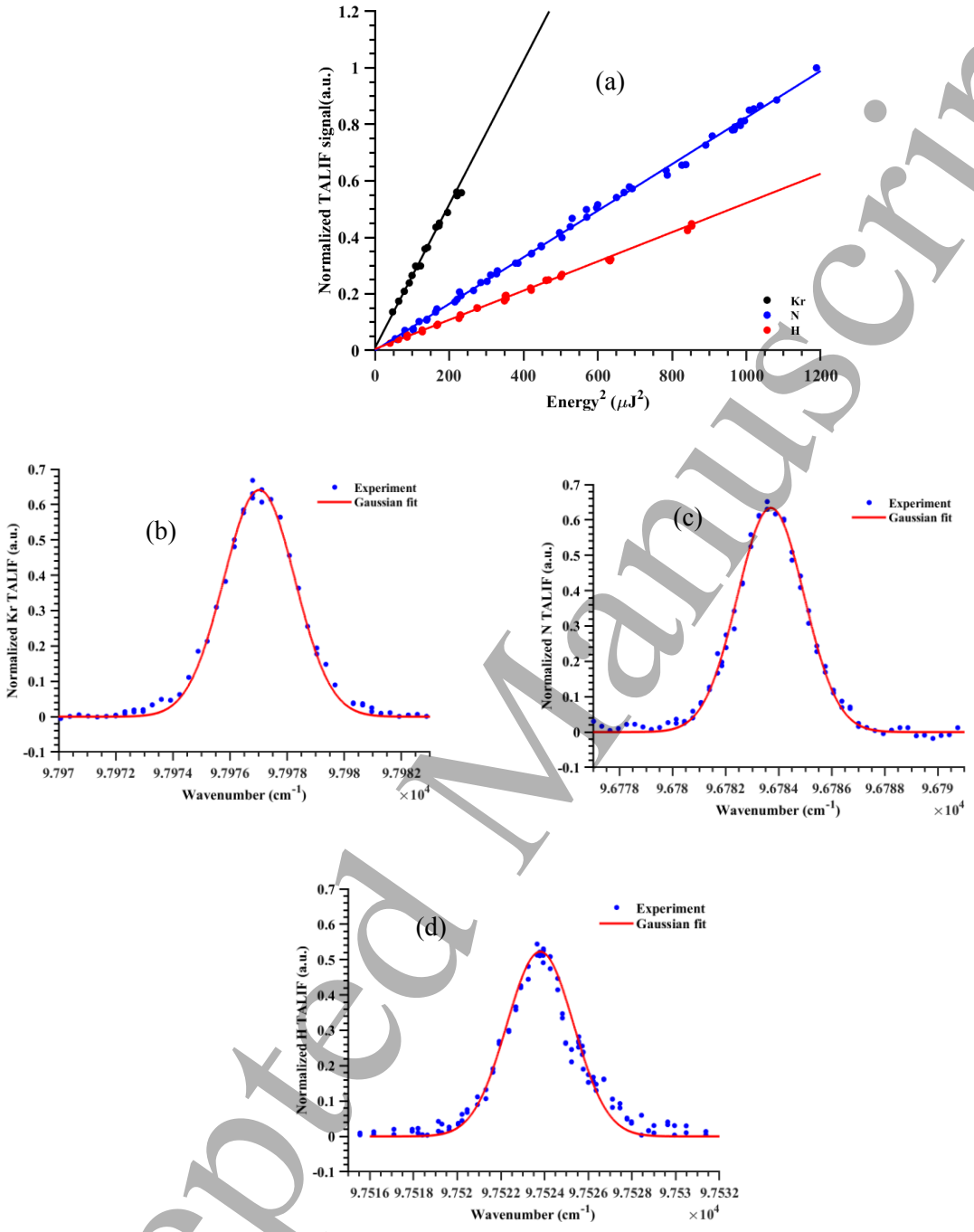

Figure 6. (a) Kr, N, and H TALIF signal versus squared laser intensity; TALIF convolution integral for (b) Kr ($5p'[3/2]_2 \rightarrow 5s'[1/2]_1$), (c) N ($3p\ ^4S_{3/2} \rightarrow 3p^4\ S_{1/2,3/2,5/2}$), and (d) H ($1s\ ^2S_{1/2} \rightarrow 3d^2\ S_{3/2,5/2}$). Kr TALIF data are taken in pure krypton at 20 Torr, N TALIF and H TALIF data are taken 100 µs after a 50-pulse discharge burst in nitrogen and 1% H_2-N_2 mixture, respectively, at 150 Torr.

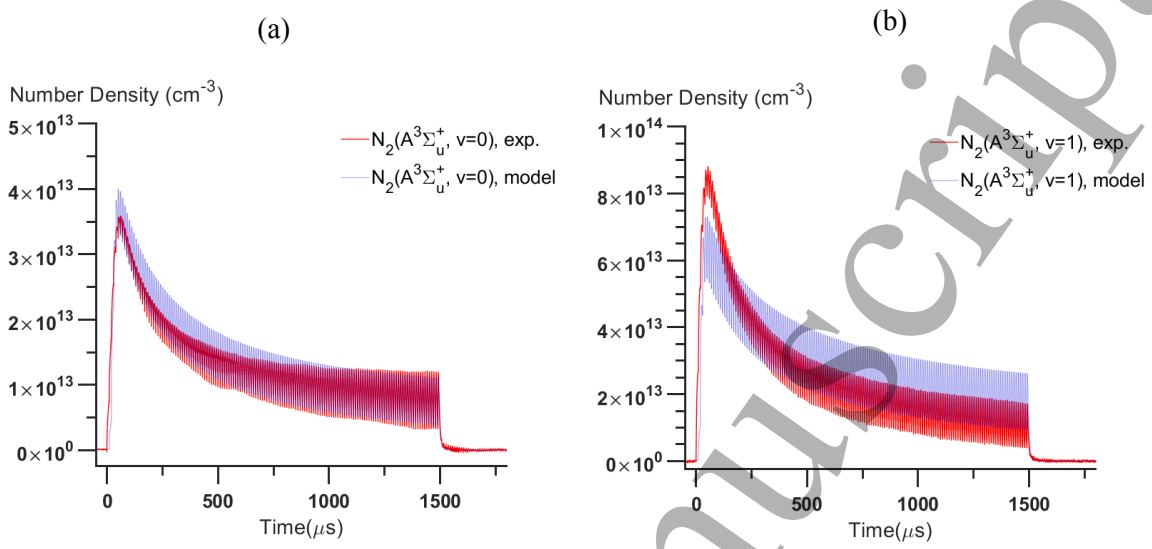

Figure 7. Time-resolved absolute (a) $N_2(A^3\Sigma_u^+,v=0)$ and (b) $N_2(A^3\Sigma_u^+,v=1)$ populations during a 150-pulse discharge burst and the afterglow in nitrogen at P=150 Torr.

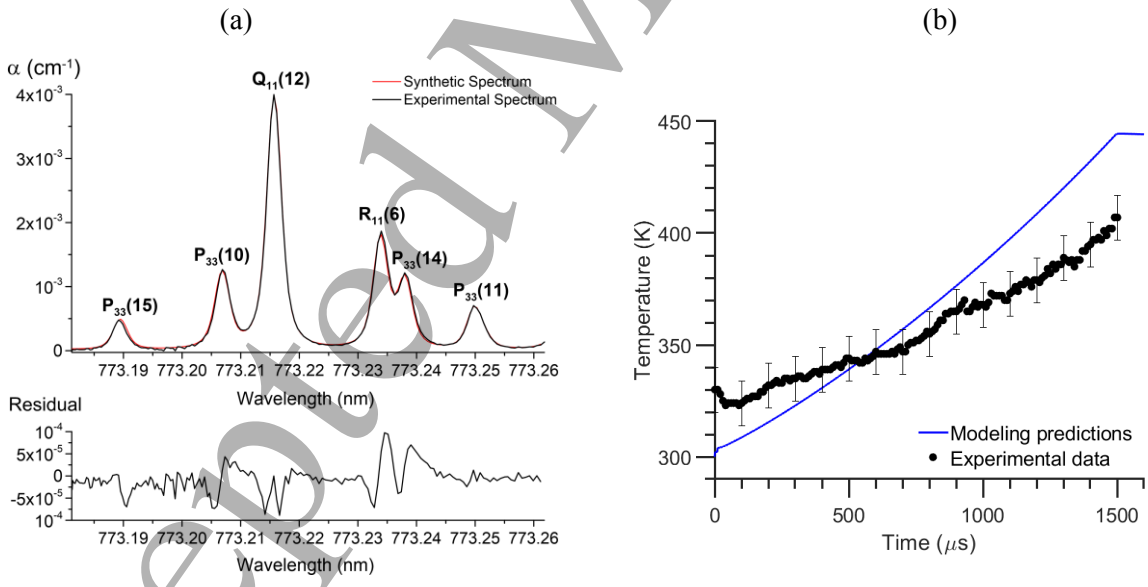

Figure 8. (a) Typical TDLAS $N_2(B^3\Pi_g,v=2 \longleftarrow A^3\Sigma_u^+,v=0)$ band spectrum compared with best fit synthetic spectrum; (b) translational-rotational temperature during a 150-pulse burst in nitrogen at P=150 Torr, compared with the modelling predictions.

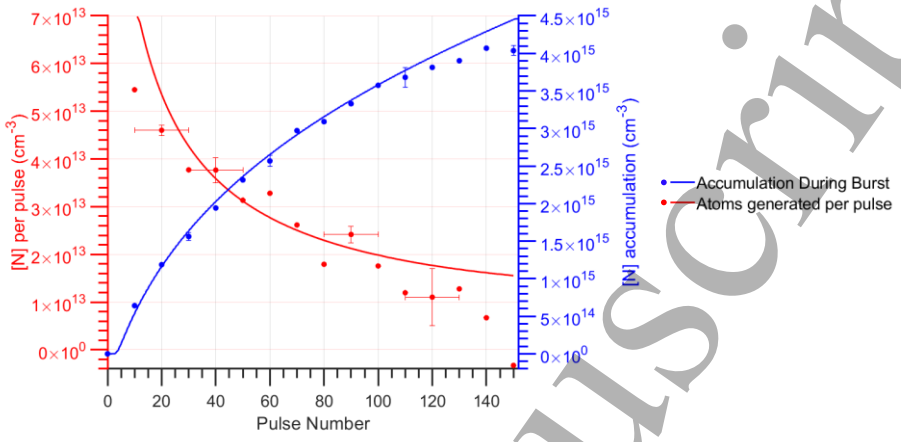

Figure 9. N atom number density (blue) and N atoms produced per pulse (red) during a 150-pulse discharge burst in nitrogen, at P=150 Torr, pulse repetition rate of 100 kHz, and burst rate of 10 Hz. The data points are taken 100 μs after each pulse. Solid lines show the modeling predictions.

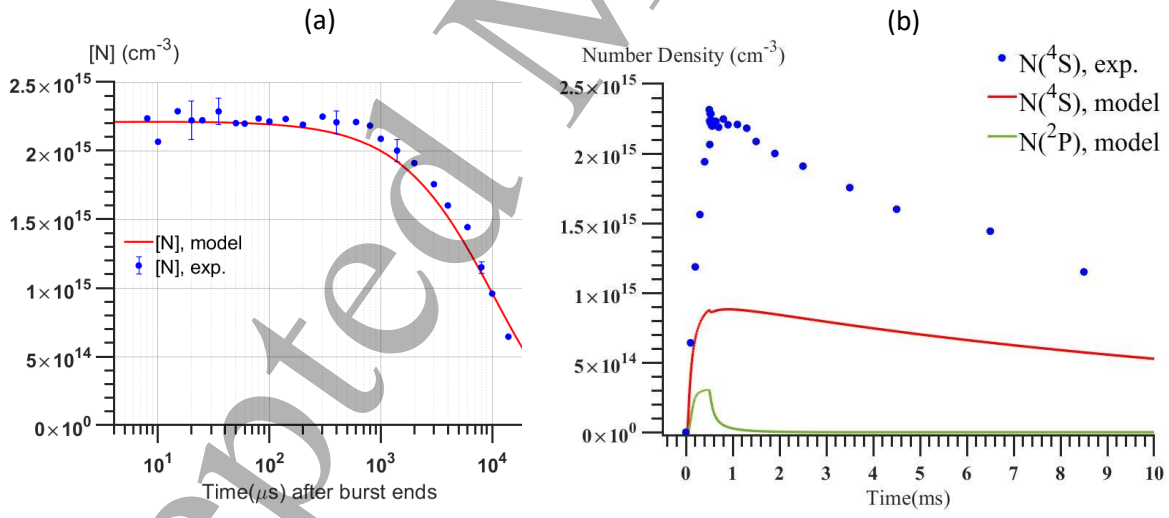

Figure 10. Time resolved N number density measured in nitrogen at P =150 Torr, for the pulse repetition rate of 100 kHz and burst rate of 10 Hz, (a) measured after the end of a 50-pulse discharge burst without generation of $N(^2P)$ atoms, and (b) measured during a 50-pulse discharge burst and its afterglow with generation of $N(^2P)$ atoms, followed by associative ionization. Solid lines show modeling predictions.

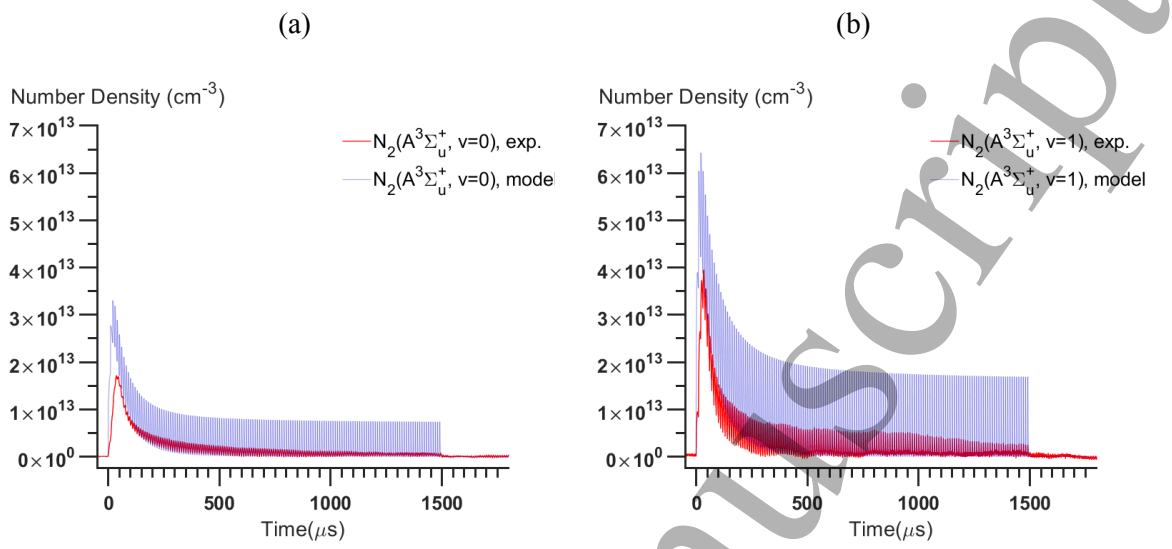

Figure 11. Time-resolved absolute (a) $N_2(A^3\Sigma_u^+, v=0)$ and (b) $N_2(A^3\Sigma_u^+, v=1)$ populations during a 150-pulse discharge burst and the afterglow in 1% H_2-N_2 at P=150 Torr. Modeling predictions are shown for the "baseline" nascent vibrational distribution of $N_2(A^3\Sigma_u^+, v)$ from Ref. [10].

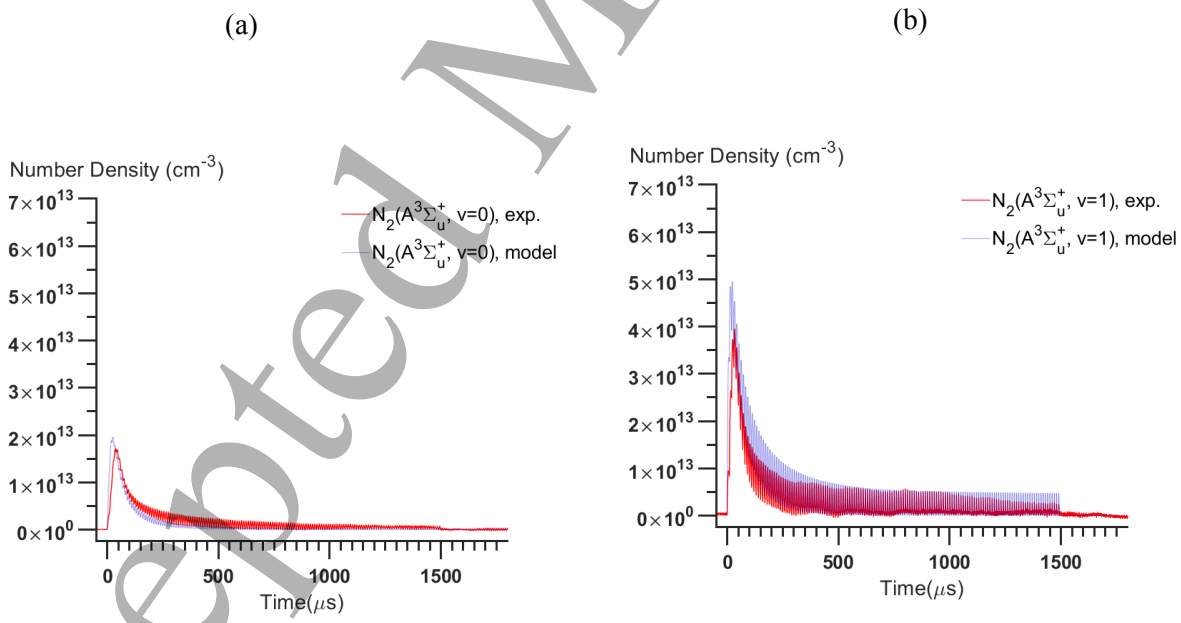

Figure 12. Time-resolved absolute (a) $N_2(A^3\Sigma_u^+, v=0)$ and (b) $N_2(A^3\Sigma_u^+, v=1)$ populations during a 150-pulse discharge burst and the afterglow in 1% H_2-N_2 at P=150 Torr. Modeling predictions are shown for the nascent vibrational distribution of $N_2(A^3\Sigma_u^+, v)$ favoring the high vibrational levels.

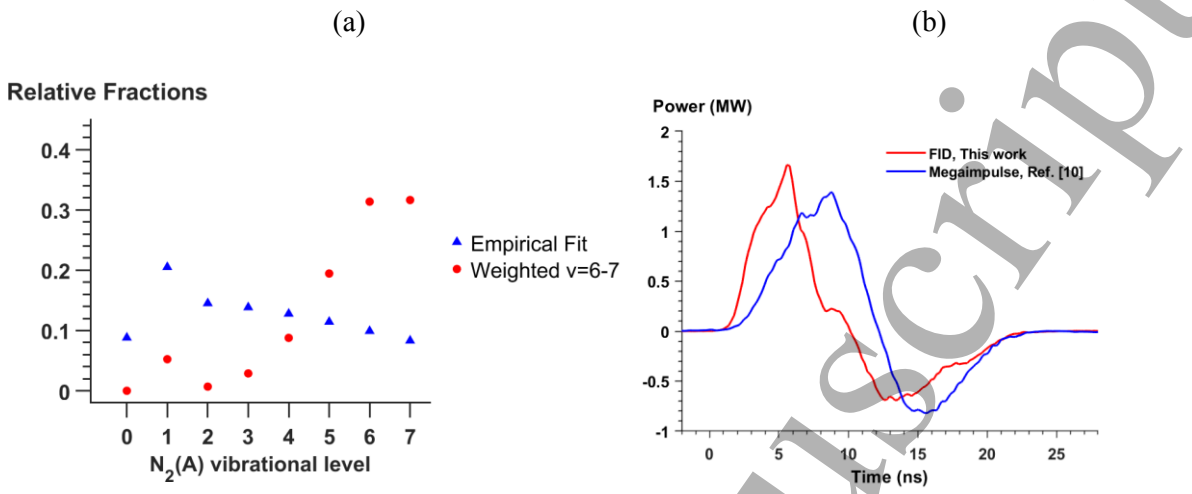

Figure 13. (a) The nascent vibrational distributions of $N_2(A^3\Sigma_u^+, v)$ used in kinetic modeling of N_2-H_2 mixtures in Fig. 11 and Fig. 12; (b) Comparison of the instantaneous power waveforms for FID 60-100MC4 pulse generator used in the present work and for MegaImpulse NPG-18/100k pulse generator used in Ref. [10].

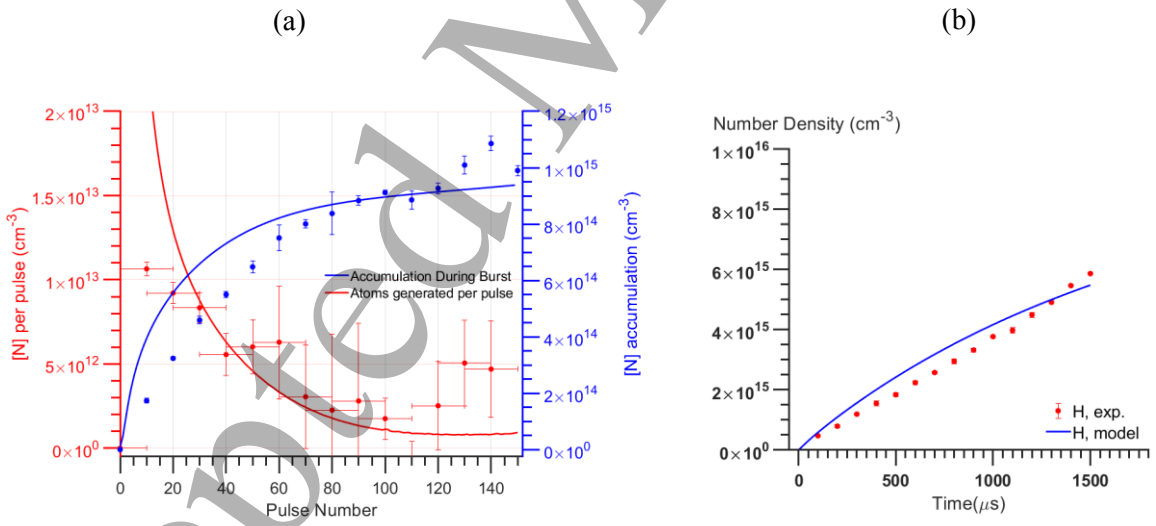

Figure 14. (a) N atom number density(blue) and N atoms produced per pulse(red) during a 150-pulse burst in 1%H_2-N_2 at P=150 Torr, at a pulse repetition rate of 100 kHz and burst rate of 10 Hz. Data points are taken 100 μs after each pulse; (b) H atoms measured at the same conditions. Solid lines show the modeling predictions.

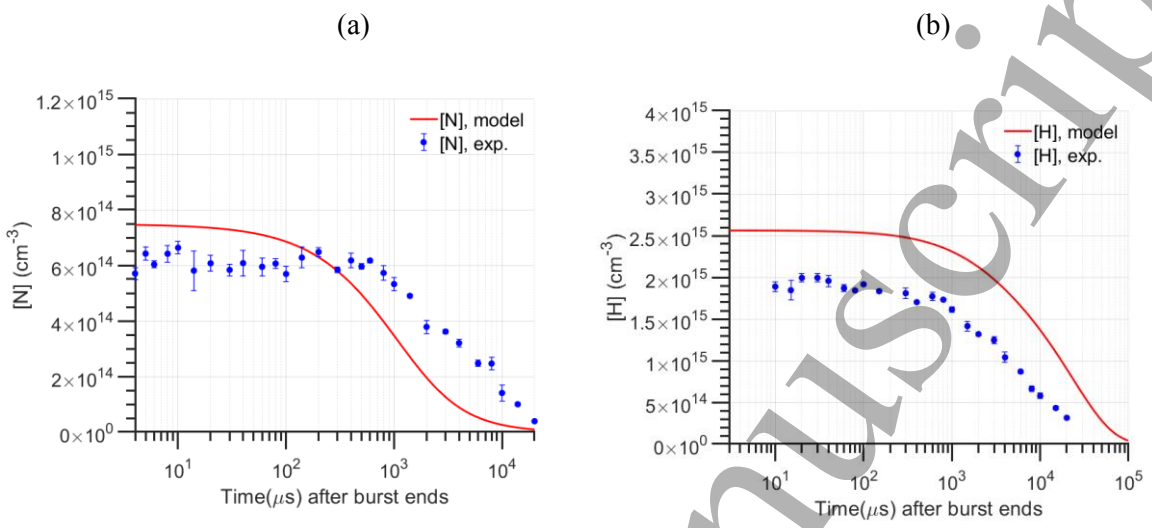

Figure 15. Time resolved number density of (a) N atoms and (b) H atoms in 1% H_2-N_2 after the end of a 50-pulse discharge burst, at a pulse repetition rate of 100 kHz and burst rate of 10 Hz. Solid lines show the modeling predictions.

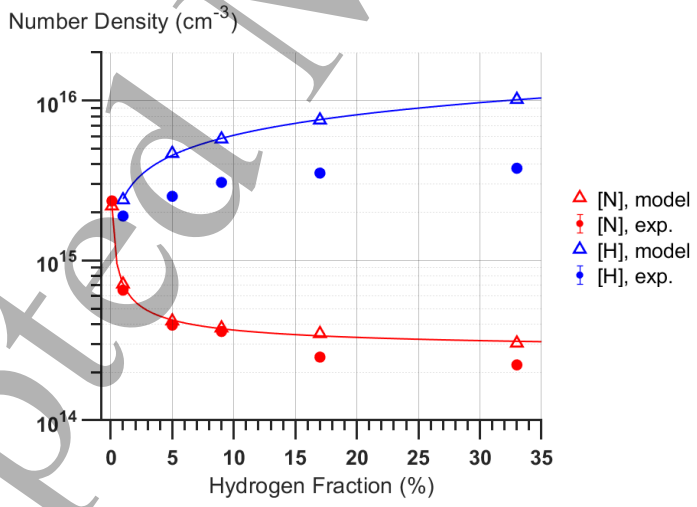

Figure 16. Number densities of N atoms and H atoms after a 50-pulse discharge burst vs. hydrogen mole fraction in the N_2-H_2 mixture. P=150 Torr, data taken 100 μs after the last pulse in the burst. Solid lines show the modeling predictions.